THE JOURNAL OF BIOLOGICAL CHEMISTRY VOL. 290, NO. 29, pp. 18134–18145, July 17, 2015

Supersaturation-limited and Unlimited Phase Transitions Compete to Produce the Pathway Complexity in Amyloid Fibrillation*

Received for publication, February 25, 2015, and in revised form, June 8, 2015 Published, JBC Papers in Press, June 10, 2015, DOI 10.1074/jbc.M115.648139

Masayuki Adachi[‡1], **Masatomo So**[‡1], **Kazumasa Sakurai**[§], **József Kardos**[¶2], **and Yuji Goto**[‡3]

From the [‡]*Institute for Protein Research, Osaka University, Yamadaoka 3-2, Suita, Osaka 565-0871, Japan,* [§]*High Pressure Protein Research Center, Institute for Advanced Technology, Kinki University, 930 Nishimitani, Kinokawa, Wakayama 649-6493, Japan, and* [¶]*Department of Biochemistry and MTA-ELTE NAP B Neuroimmunology Research Group, Eötvös Loránd University, Pázmány sétány 1/C, Budapest, 1117, Hungary*

Background: Relationship between amyloid fibrils and amorphous aggregates has not yet been elucidated.
Results: A competitive mechanism of amyloid fibrillation and amorphous aggregation reproduced the observed aggregation kinetics of β_2-microglobulin.
Conclusion: Apparent complexities in amyloid fibrillation are explained assuming supersaturation-limited crystal-like amyloid fibrils and unlimited glass-like amorphous aggregates.
Significance: Linkage of the kinetics of protein aggregation and a conformational phase diagram improves the understanding of protein aggregation.

Although amyloid fibrils and amorphous aggregates are two types of aggregates formed by denatured proteins, their relationship currently remains unclear. We used β_2-microglobulin (β2m), a protein responsible for dialysis-related amyloidosis, to clarify the mechanism by which proteins form either amyloid fibrils or amorphous aggregates. When ultrasonication was used to accelerate the spontaneous fibrillation of β2m at pH 2.0, the effects observed depended on ultrasonic power; although stronger ultrasonic power effectively accelerated fibrillation, excessively strong ultrasonic power decreased the amount of fibrils formed, as monitored by thioflavin T fluorescence. An analysis of the products formed indicated that excessively strong ultrasonic power generated fibrillar aggregates that retained β-structures but without high efficiency as seeds. On the other hand, when the spontaneous fibrillation of β2m was induced at higher concentrations of NaCl at pH 2.0 with stirring, amorphous aggregates became more dominant than amyloid fibrils. These apparent complexities in fibrillation were explained comprehensively by a competitive mechanism in which supersaturation-limited reactions competed with supersaturation-unlimited reactions. We link the kinetics of protein aggregation and a conformational phase diagram, in which supersaturation played important roles.

The aggregates of denatured proteins were classified into two types; amyloid fibrils and amorphous aggregates. Amyloid fibrils are fibrillar aggregates with a width of ~10 nm and length of several micrometers (1–3). The dominant secondary structure is a cross-β structure stabilized by an ordered hydrogen bond network. Although they were found to be associated with >30 types of amyloidoses, including dialysis-related amyloidosis caused by β_2-microglobulin (β2m)[4] (4), various proteins not associated with diseases have also been shown to form amyloid fibrils, indicating that amyloid fibrillation is a generic property of denatured proteins (1). Previous studies proposed that amyloid fibrils formed in the supersaturated solutions of precursor proteins through a nucleation and growth mechanism that was characterized by a lag phase or via seed-dependent growth without a lag phase (5–7). We revisited "supersaturation" and argued its critical involvement in amyloid fibrillation (8–12). It is noted that the role of supersaturation in the kinetics and thermodynamics of fiber formation of hemoglobin S, which is associated with sickle cell anemia, has been studied extensively (13, 14). The role of supersaturation at the proteome level in neurodegenerative diseases has recently been reported (15).

On the other hand, the term amorphous aggregate has been collectively used for other types of aggregates (16), which have not been the targets of intensive research. We previously suggested that amyloid fibrils and amorphous aggregates were similar to the crystals and glasses of substances, respectively (8), and that they are represented by the same phase diagram as often used for crystallization of substances (Fig. 1*A*). Nevertheless, the relationship between amyloid fibrils, amorphous aggregates, and related aggregates such as oligomers or curvilinear fibrils has not yet been elucidated in detail (16, 17). One of the most important issues for clarifying the mechanism of protein aggregation is whether amorphous aggregates including

* This work was supported by the Japanese Ministry of Education, Culture, Sports, Science, and Technology and performed under the International Collaborative Research Program of Institute for Protein Research, Osaka University. The authors declare that they have no conflicts of interest with the contents of this article.
[1] Both authors contributed equally to this work.
[2] Supported by the Hungarian National Research, Development and Innovation Office (KTIA_NAP_13-2-2014-0017).
[3] To whom correspondence should be addressed. Tel.: 81-6-6879-8614; Fax: 81-6-6879-8616; E-mail: ygoto@protein.osaka-u.ac.jp.

[4] The abbreviations used are: β2m, β_2-microglobulin; AFM, atomic force microscopy; TEM, transmission electron microscopy; ThT, thioflavin T; ANS, 1-anilino-8-naphthalenesulfonate.

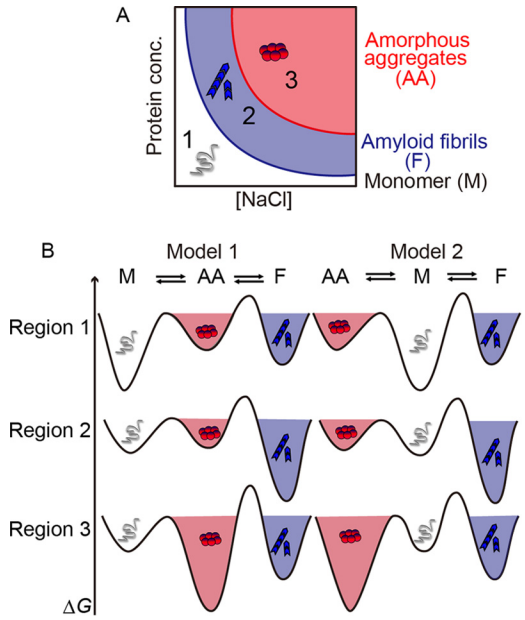

FIGURE 1. **General phase diagram for the conformational transitions of proteins.** *A*, salt- and protein concentration-dependent conformational phase diagram of β2m under acidic conditions is illustrated. The regions of unfolded monomers (*Region 1*), amyloid fibrils (*Region 2*), and amorphous aggregates (*Region 3*) are shown. *B*, relative free energies of monomers (*M*), amorphous aggregates (*AA*), and amyloid fibrils (*F*) under distinct regions of phase diagram are compared between a consecutive model (*Model 1*) with on-pathway AA and competitive model (*Model 2*) with off-pathway AA. Free energy barriers between the conformational states are also included assuming that the barriers for amyloid fibrils are higher than those for amorphous aggregates.

oligomers or protofibrils represent on-pathway intermediates leading to amyloid fibrils or off-pathway dead products (Fig. 1*B*).

Various kinds of agitations such as shaking (18), stirring (19), or ultrasonic irradiation (8, 20–23) have been shown to effectively force spontaneous fibrillation under conditions in which no fibrillation was expected because of the persistent metastability of supersaturation. In the case of ultrasonication-forced fibrillation, we suggested that interactions with the hydrophobic surfaces of cavitation bubbles condensed proteins, leading to the breakdown of supersaturation and then fibrillation (8, 23). Ultrasonication is now recognized as one of the important approaches for elucidating the mechanisms underlying amyloid fibrillation (23–25).

When we monitored the ultrasonication-dependent fibrillation of proteins by thioflavin T (ThT), we often observed a significant decrease in ThT fluorescence after the burst-phase increase (22, 25–27). The decrease in ThT fluorescence was accelerated when the lag time was shorter, suggesting that this reduction was caused by the ultrasonication-dependent transformation of preformed fibrils into distinct conformational states (22, 25, 26). Combined with the salt concentration-dependent competition between fibrillation and amorphous aggregation, we showed that a competitive mechanism, in which various amyloidogenic and non-amyloidogenic aggregates competed (Fig. 1*B*, *Model 2*), explained comprehensively the kinetics and thermodynamics of protein aggregation.

Experimental Procedures

Proteins and Chemicals—A recombinant human β2m protein with an additional methionine residue at the N terminus was expressed in *Escherichia coli* and purified as previously reported (28). ThT was obtained from Wako Pure Chemical Industries, Ltd. (Osaka, Japan). All other reagents were purchased from Nacalai Tesque (Kyoto, Japan).

Amyloid Fibrillation under Ultrasonication—Lyophilized β2m was dissolved in 10 mM HCl. The concentration of β2m was determined spectrophotometrically using a molar extinction coefficient of 19,300 M^{-1} cm^{-1} at 280 nm based on its amino acid composition. The sample solution of 1 ml in a disposable cuvette with a 1-cm light path contained 25 μM β2m, 0.1 M NaCl, 5 μM ThT, and 10 mM HCl. We used a water bath-type ultrasonic transmitter with a temperature controller (ELESTEIN, Elekon Science Co., Chiba, Japan) to induce fibrillation (20, 22). A cycle involving 1 min of ultrasonication and 9 min of quiescence was repeated. The temperature of the water bath was set to 37 °C.

We measured temperature increases due to ultrasonication with a thermocouple (Compact Thermologger AM-8000K, Anritsu, Tokyo, Japan) to monitor the strength of ultrasonication. Among the several methods employed to determine ultrasonic power, calorimetry is often used to specify the ultrasonic power dissipated into a solution, in which the initial rate of the temperature increase is measured upon irradiation of the solution with ultrasonic pulses (24). With the calorimetric method, ultrasonic power (Q) was calculated using the equation: $Q = (dT/dt)C_pM$, where C_p is the heat capacity of water (4.2 $Jg^{-1}K^{-1}$), M is the mass of water (g), and (dT/dt) is the increase in temperature per second. In other words, with the same sample volumes, dT/dt was proportional to ultrasonic power.

Amyloid fibrillation was detected by ThT fluorescence with an excitation wavelength of 445 nm and emission wavelength of 485 nm using the Hitachi fluorescence spectrophotometer F7000 or F4500 (Tokyo, Japan). ANS fluorescence was also monitored with the same fluorometers with an excitation wavelength of 350 nm and emission wavelength of 485 nm.

The seeding experiments were performed by adding 5% (v/v) seeds to the monomeric β2m solution. Seed fibrils were prepared by ultrasonication as described above. Kinetics were monitored using a SH9000 microplate reader (Corona Electric. Co., Ibaraki, Japan).

Amyloid Fibrillation in the Presence of NaCl—The sample solution of 2 ml in a glass cuvette with a 1-cm light path contained 25 μM β2m, 5 μM ThT, 50 μM ANS, 10 mM HCl, and various concentrations of NaCl. ThT and ANS fluorescence under stirring with a stirring bar was measured with the F7000 fluorescence spectrometer. Excitation and emission wavelengths were the same as those described above.

Circular Dichroism, Atomic Force Microscopy (AFM), and Transmission Electron Microscopy (TEM) Measurements—Far-UV CD spectra were measured with a Jasco J720 spectropolarimeter (Tokyo, Japan) as described previously (20). Measurements were performed at 25 °C using a quartz cuvette with a 1-mm path length, and the results were expressed as mean residue ellipticity [θ].

AFM images were obtained using a Digital Instruments Nanoscope IIIa scanning microscope (Veeco Instruments Inc., Plainview, NY) as described previously (25). Regarding TEM measurements, 10-fold diluted samples were spotted onto a collodion-coated copper grid (Nisshin EM Co., Tokyo, Japan). After 1 min, the remaining solution was removed with filter paper, and 5 μl 2% (w/w) ammonium molybdate was spotted. After 1 min, the remaining solution was removed in the same manner. TEM (Hitachi H-7650, Tokyo, Japan) images were obtained at 20 °C with a voltage of 80 kV and magnification of 20,000.

Fourier Transform Infrared Spectroscopy—FTIR measurements were carried out on a Bruker Equinox 55 (Bruker, Germany) instrument equipped with an MCT detector in CaF_2 cells with 100 μm Teflon spacers at 1 cm^{-1} resolution as described previously (11). To avoid the contribution of water vapor peaks to the spectra, the instrument was purged with dry air. Native and acid unfolded monomeric β2m solutions were prepared by dissolving the lyophilized β2m powder in D_2O solutions containing 10 mM sodium phosphate, 0.1 M NaCl, pD 7.5, or ~10 mM DCl, 0.1 M NaCl, respectively.

Amyloid fibrils were induced in a disposable cuvette with a 1-cm light path by stirring or with the same cycles of ultrasonication and quiescence. Then, fibrillar samples were concentrated by centrifugation for 30 min at 40,000 rpm with a Beckman TL-100 ultracentrifuge using a TLA100.3 rotor. The supernatant was used as a background reference.

The spectra shown were baseline-subtracted, corrected for vapor and HDO contamination, and normalized to an area that is approximately equal to that of a 5 mg/ml protein solution. The second derivative of the spectra was used to determine the positions of the components (30). The fitting was performed by fitting Gaussian functions to the original curve. The width of the Gaussian curves was limited to <20 cm^{-1}. Components at 1585, 1600, and 1612 cm^{-1} and above 1700 cm^{-1} are considered as side chain signals. The secondary structure content (%) was calculated from the area of the fitted components.

Results

Ultrasonication-forced Amyloid Fibrillation—We examined the dependence of β2m fibrillation on ultrasonic power by using different positions of the ultrasonicator bath. Amyloid fibrillation was monitored by ThT fluorescence at 485 nm (Fig. 2*A*). We simultaneously monitored ultrasonic power by measuring temperature increases in the sample solution (Fig. 2*B*). With cycles of 1 min of ultrasonication and 9 min of quiescence, the marked increase observed in temperature during ultrasonic irradiation was followed by a slightly slower decrease in temperature, and a constant temperature was maintained for 5 min. We assumed that the maximal increase in temperature was approximately proportional to (dT/dt) and, thus, ultrasonic power.

Distinct kinetics were observed depending on ultrasonic power (Fig. 2, *A–C*). When ultrasonic power was weak, as represented by a small increase in temperature (*i.e.* 4 °C), the amyloid burst occurred after a lag time of 4 h. With increasing ultrasonic power (*i.e.* a temperature increase of 7 °C), the lag time was shortened to 2 h and accompanied by a decrease in the maximal ThT fluorescence. A gradual decrease in ThT fluorescence was then observed (Fig. 2*A*). When fibrillation was monitored under strong ultrasonic power (*i.e.* a temperature increase of 17 °C), the lag time was further shortened to 1 h and accompanied by only a small increase in ThT fluorescence followed by a subsequent decrease. These ultrasonic power-dependent decreases in the lag time and ThT fluorescence (Fig. 2*C*) were consistent with our previous studies on β2m (22, 25) and findings on α-synuclein fibrils (27) and amyloid β-(1–40) fibrils (26), implying that extensive ultrasonication transformed the preformed fibrils to amorphous aggregates. In addition, the decrease observed in maximal ThT fluorescence with an increase in ultrasonic power suggested the direct formation of amorphous aggregates as well as amyloid fibrils. However, this was not the case for β2m, as will be described later.

Here, to check the effects of an increase in temperature on fibrillation, spontaneous fibrillation of 25 μM β2m in 0.1 M NaCl, 5 μM ThT, and 10 mM HCl was monitored in the presence or absence of stirring at several temperatures using the Hitachi fluorescence spectrophotometer F4500 (Fig. 2*D*). The stirring accelerated the fibrillation, and higher temperature slightly increased the rate of fibrillation. However, without stirring, no fibrillation occurred even after 6 h at any temperatures. The intrinsic decrease in ThT fluorescence upon increasing the temperature caused the decrease in the final ThT fluorescence. In our ultrasonication experiments, the increase in temperature occurred only transiently (Fig. 2*B*), and the stirring effects caused by ultrasonic irradiation may not be significant. Thus, although ultrasonication is linked with the increase in temperature and the increase in temperature may be one of the important factors accelerating fibrillation, we do not consider that the increase in temperature is a major driving force of amyloid fibrillation, and fibrillation is dominantly accelerated by ultrasonication-dependent cavitation.

Morphologies and Secondary Structures of Ultrasonication-induced Products—We analyzed the morphologies of ultrasonication-induced products by AFM and TEM. Under the condition of weak ultrasonic power, typical short fibrils were produced after the lag time and were further fragmented by extensive ultrasonication (Fig. 2, *G–I*). Although similar morphological changes were observed under the condition of stronger ultrasonic power, amyloid particles were finer than those under weaker ultrasonic power (Fig. 2, *J* and *K*). The formation of amorphous aggregates was unclear; however, we sometimes observed clumps, suggesting amorphous aggregates.

We examined the secondary structures by measuring far UV CD spectra (Fig. 2, *E* and *F*). β2m monomers were largely disordered at pH 2.0 in 10 mM HCl and 0.1 M NaCl. After the ThT burst induced by the ultrasonic irradiation of weak power, transformation to the spectrum of a typical β-sheet structure was observed (Fig. 2*F*). Similar changes in the spectrum were observed even under the conditions of strong ultrasonic power in which only a slight increase in ThT fluorescence was noted (Fig. 2*E*). These results suggested that, in the case of β2m, strong ultrasonic power induced "amyloid-like" β structures without strong ThT fluorescence. Although further ultrasonication decreased ThT fluorescence, the CD spectrum of the β-sheet structure remained, indicating that extensive ultra-

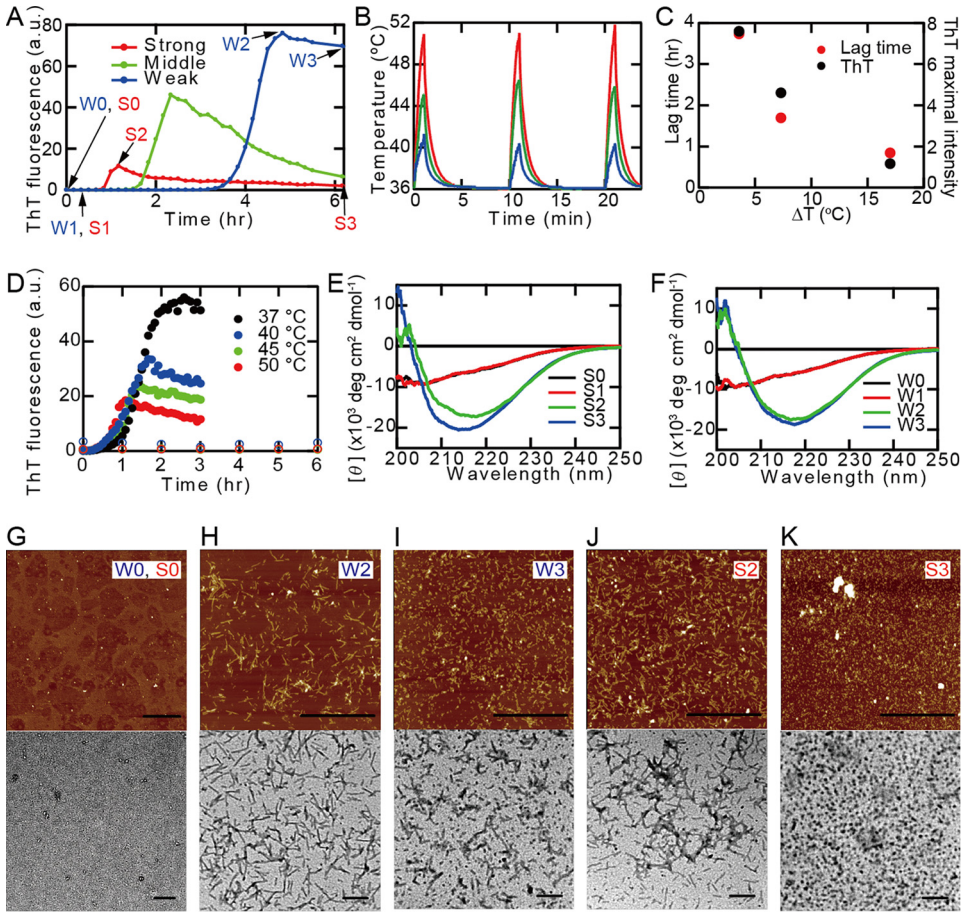

FIGURE 2. **Ultrasonication-forced amyloid fibrillation of β2m under various levels of ultrasonic power.** *A*, fibrillation kinetics of 25 μM β2m at 10 mM HCl, 0.1 M NaCl, and 5 μM ThT monitored by ThT fluorescence at 485 nm. *a.u.*, arbitrary units; *S*, strong; *W*, weak. *B*, change in temperature during cycles of 1 min of ultrasonication and 9 min of quiescence under various levels of ultrasonic power as monitored by a thermocouple. The temperature of the water bath was set to 37 °C. *C*, the dependence of the lag time on temperature increases. *D*, fibrillation kinetics at various temperatures in the presence (*solid symbols*) or absence (*open symbols*) of stirring directly monitored using the fluorescence spectrophotometer. Fluorescence intensities in *A* and *D* cannot be compared because of the difference in settings. *E* and *F*, CD spectra of samples under strong (*E*) and weak (*F*) ultrasonic power. *G–K*, AFM and TEM images of aggregates formed under weak (*G–I*) and strong (*J* and *K*) ultrasonic power. The time points for preparation of samples shown in panels (*E–K*) were indicated in *A*. The *scale bars* on the AFM and TEM images indicate 1 μm and 200 nm, respectively.

sonic irradiation to the preformed fibrils did not destroy the β-sheet structure. These results were distinct from those for α-synuclein (27) or amyloid β-(1–40) (26), in which strong ultrasonic irradiation to the preformed fibrils changed the CD spectra from those of β-structures to those of highly disordered structures.

We then used FTIR to examine the secondary structures of fibrillar aggregates as well as other conformational states (Table 1 and Fig. 3). The advantages of FTIR spectroscopy are that β-sheet structures can be distinguished from other structures more clearly than by CD (30, 32) and that antiparallel β-structures can also be identified, depending on the presence of a small but sharp high frequency peak at 1690–1695 cm^{-1} in non-deuterated and at 1682–1685 cm^{-1} in deuterated form (30).

Native β2m showed β components around 1636 and 1690 cm^{-1} that are related to antiparallel β structures. In contrast, acid denatured β2m was proven to be largely disordered. In most of the fibril samples, we observed the dominant intermolecular β components appearing at 1620–1622 cm^{-1} accompanied by minor, native-like β components around 1632–1636 cm^{-1}. The intermolecular β components may represent parallel β structures considering the absence of a clear high frequency peak. We have to note that the fibrils formed under strong sonication tended to contain visible large aggregates. Their spectral amplitudes were lower, and the spectra were noisier, probably because of inhomogeneity of the samples.

Taken together, the FTIR spectra of ultrasonicated fibrils were consistent with the CD spectra indicating that, although the strong ultrasonic irradiation did not produce fibrils with marked ThT fluorescence, fibrils with secondary structures similar to those of mature amyloid fibrils were formed.

ANS Binding and Size Distribution of Ultrasonication-induced Products—ANS is an amphiphilic fluorescence dye that specifically interacts with the water-accessible hydrophobic surface of proteins (27, 33). We examined the interaction of ANS with amyloid fibrils and their products formed by extensive ultrasonication with different levels of ultrasonic power (Fig. 4*B*). Under both strong and weak ultrasonic power, ANS fluorescence increased with the formation of amyloid fibrils and decreased with further ultrasonic irradiation (data not shown). The rate of the decrease was accelerated under the stronger ultrasonic power. The kinetics of the increase and

TABLE 1

Secondary structure assignments of various conformational states of β2m on the basis of FTIR spectra

Experiments were carried out in D_2O solutions, and pD is the pH meter reading in D_2O.

Conformation (conditions)	Major components	Wave number	Fraction	Structure assignment
		cm^{-1}	%	
Native (pD 7.5)	Antiparallel β-sheet	1636	48	β
		1646	18	Random
		1659	15	Turn
		1673	18	Turn
		1690	1.4	High frequency antiparallel β
Acid denatured (pD 2.0, 0.1 M NaCl)	Disordered	1632	1	β
		1640	68	Random
		1668	31	Turn
		1693	0.1	High frequency antiparallel β
Fibrils formed by stirring (pD 2.0, 0.1 M NaCl)	Parallel β-sheet	1620	41	β
		1634	10	β
		1644	22	Random
		1661	21	Turn
		1683	5	Turn/high frequency Antiparallel β
Amorphous aggregates (pD 2.0, 1.0 M NaCl)	Antiparallel β-sheet	1616	19	β
		1634	40	β
		1650	6	Random/helix
		1664	31	Turn
		1685	3	High frequency antiparallel β
Fibrils formed under strong sonication (pD 2.0, 0.1 M NaCl)	Parallel β-sheet	1621	34	β
		1636	14	β
		1649	19	Random
		1664	19	Turn
		1681	14	Turn/high frequency antiparallel β?
Fibrils formed under weak sonication (pD 2.0, 0.1 M NaCl)	Parallel β-sheet	1620	27	β
		1632	37	β
		1649	14	Random
		1662	18	Turn
		1682	3	Turn/high frequency Antiparallel β?
Strongly sonicated fibrils after formation by weak sonication (pD 2.0, 0.1 M NaCl)	Parallel β-sheet	1622	38	β
		1635	15	β
		1648	24	Random
		1664	18	Turn
		1685	5	Turn/high frequency antiparallel β?

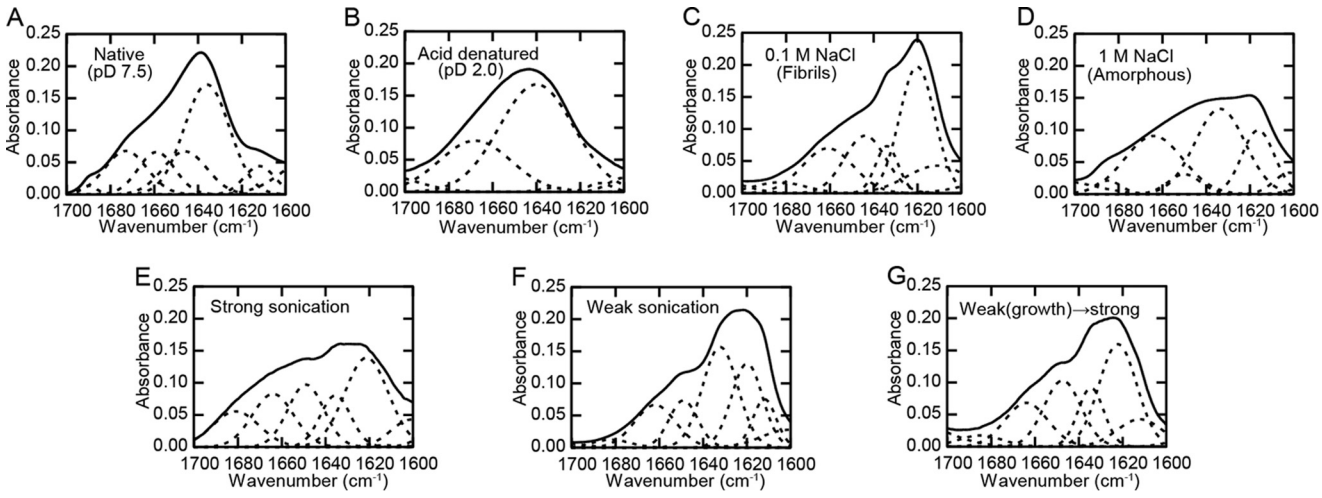

FIGURE 3. **FTIR spectra of various conformational states of β2m in 10 mM DCl and D_2O.** *A*, the native state of β2m at, as the exception, pD 7.5, in 10 mM sodium phosphate, 0.1 M NaCl. *B*, the acid-denatured monomer state. *C*, amyloid fibrils formed in 0.1 M NaCl. *D*, amorphous aggregates in 1.0 M NaCl. *E* and *F*, fibril samples prepared under strong (*E*) and weak (*F*) ultrasonic power, respectively. *G*, extensively ultrasonicated fibrils after fibrillation under weak ultrasonic power. The *solid lines* represent the raw data, and *broken lines* represent the deconvoluted spectra. The fitted spectra (not shown) on the basis of deconvoluted spectra were practically the same as the raw data.

decrease in ANS fluorescence were similar to those of ThT fluorescence, suggesting that the change in the binding regions for ThT and ANS occurred simultaneously.

Considering the possibility that decreases in ANS or ThT fluorescence occurred by the chemical decomposition of the dyes, we added ANS or ThT to samples with decreased fluorescence intensities (Fig. 4, *A* and *B*). However, no increase was observed in ANS or ThT fluorescence, confirming that the decreases in ANS or ThT fluorescence were not caused by the decomposition of dyes. These results suggested that extensive ultrasonication decreased the ANS-specific exposed hydrophobic surfaces of fibrils as well as the amyloid-specific surfaces detected by ThT.

We investigated the size distribution of the extensively ultrasonicated products by analytical ultracentrifugation (Fig. 4, *C* and *D*). The distribution of sedimentation coefficient (*s*) was

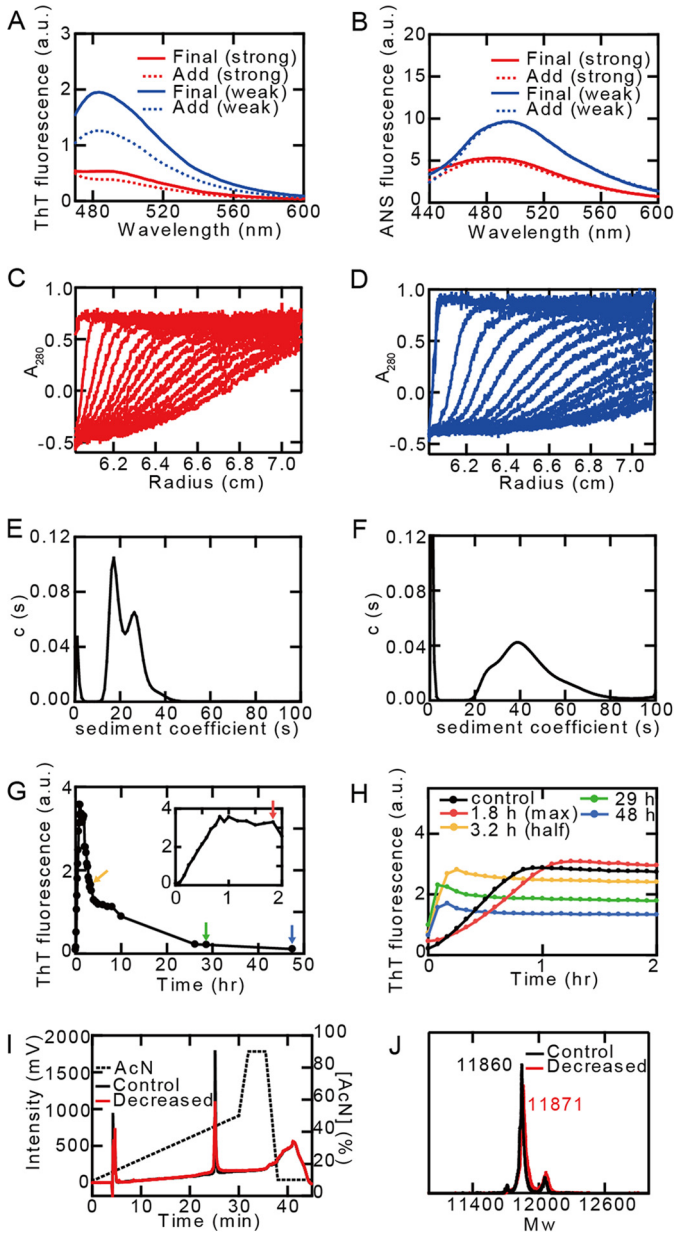

FIGURE 4. **Analysis of ultrasonication-induced products.** *A* and *B*, fluorescence spectra to monitor the effects of additional ThT (*A*) or ANS (*B*) on samples of reduced fluorescence intensities under strong and weak ultrasonic power. *a.u.*, arbitrary units. *C* and *D*, boundary curves of sedimentation velocity for products under strong (*C*) and weak (*D*) ultrasonic power. *E* and *F*, sedimentation coefficient (*c(s)*) distributions derived from sedimentation boundary profiles under strong (*E*) and weak (*F*) ultrasonic power. *G*, ultrasonication-forced fibrillation to prepare seed fibrils monitored by ThT fluorescence at 485 nm. The *inset* indicates expanded kinetics within 2 h. The sample solution contained 25 μM β2m, 0.1 M NaCl, 5 μM ThT, and 10 mM HCl. *H*, seeding reactions with seed fibrils (5% (v/v)) obtained at various stages of fibrillation, as shown in *G*. *I* and *J*, effects of extensive ultrasonication on chemical structures of β2m. Extensively ultrasonicated fibrils with decreased ThT fluorescence were analyzed by reverse-phased HPLC (*I*) and mass spectrometry (*J*) after depolymerization by 4 M guanidine-HCl.

estimated from the boundary curves of sedimentation velocity using sedfit software. As for the products under strong ultrasonic power, *s* values were distributed with two maxima at 18 and 27 s (Fig. 4*E*). On the other hand, regarding the products under weak ultrasonic power, *s* values were distributed with a broad maximum at 43 s (Fig. 4*F*). Thus, the sizes of aggregates appeared to be larger under the weaker ultrasonic power, which is consistent with the AFM or TEM measurements (Fig. 2). The strongly sonicated fibrils with components of 18 and 27 s were considered to have solubility of the former higher than the latter and higher than that of fibrils grown under weak sonication.

To further explore the effects of the extensive ultrasonication of preformed fibrils, we performed seeding experiments using fibrils at various stages of decreases in ThT fluorescence (Fig. 4, *G* and *H*). When seed fibrils with almost no ThT fluorescence were used, the final ThT intensity was ~50% that of the control fibrils, although the reaction was accelerated. These faster reactions were caused by the ultrasonication-induced fragmentation of fibrils. On the other hand, the decrease observed in the ThT intensity suggested that the seed fibrils trapped the monomers to prevent further fibrillation. Thus, extensively ultrasonicated fibrils may reduce the potential of efficient seeds.

We also examined the effects of extensive ultrasonication on the chemical structures of β2m (Fig. 4, *I* and *J*). An analysis with the reverse-phased HPLC showed that β2m monomers depolymerized from fibrils with decreased ThT fluorescence by 4 M guanidine HCl had the same retention time as that of the control monomers. An analysis with mass spectrometry confirmed the intactness of β2m molecules depolymerized from fibrils. Thus, the marked decreases observed in ThT fluorescence were not caused by the chemical decomposition of β2m molecules.

Salt-dependent Fibrillation and Aggregation—We previously showed that, although fibrillation was accelerated by low concentrations of NaCl of ~0.1 M, concentrations higher than 0.5 M inhibited fibrillation and induced amorphous aggregates (8, 34). To compare the products produced in the presence of high salt levels and extensive ultrasonication, we examined NaCl concentration-dependent competition between fibrillation and amorphous aggregation. Amyloid fibrillation in the presence of various concentrations of NaCl in 10 mM HCl was monitored by ThT and ANS fluorescence (Fig. 5, *A*–*H*).

No significant change was observed in ThT in the absence of NaCl; however, a small increase in ANS fluorescence was noted within the dead time of the measurements (*i.e.* ~20 s). Burst increases in ThT and ANS fluorescence were observed in the presence of 0.05 M NaCl after a lag time of 2.5 h. The marked increase in ANS fluorescence at 0.05 M was attributed to electrostatic attractions between negatively charged ANS and positively charged amyloid fibrils (see below). The lag time became shorter with increases in the concentration of NaCl. At 0.3 M NaCl, we clearly observed two-step kinetics monitored by ANS, whereas ThT fluorescence showed typical kinetics with a lag time of 0.5 h. At 0.4 M NaCl, ANS fluorescence showed fast and major saturating kinetics followed by slow and small increases in ThT fluorescence. Only a very rapid increase in ANS fluorescence was observed at 1.0 M NaCl.

The end products at various concentrations of NaCl were examined by far-UV CD (Fig. 5*I*). In the absence of NaCl, the spectrum showed a largely disordered conformation. Typical β-structures were observed at 0.05 and 0.1 M NaCl. At NaCl concentrations higher than 0.2 M, the CD intensity decreased due to the precipitation of aggregates. We previously reported that the main products at higher concentrations of

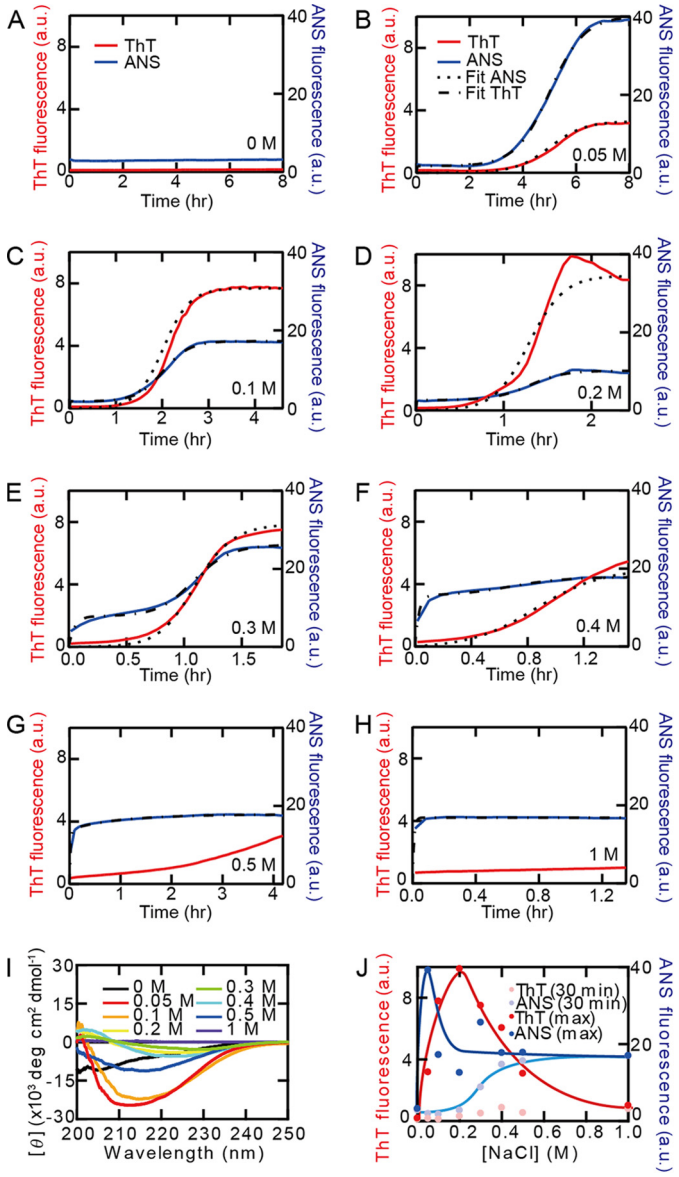

FIGURE 5. **Dependence of amyloid fibrillation of β2m on the NaCl concentration.** The kinetics of protein aggregation in 10 mM HCl at 37 °C were measured by observing ThT fluorescence at 485 nm (*red*) and ANS (*blue*) fluorescence at 485 nm. NaCl concentrations were 0 (*A*), 0.05 (*B*), 0.1 (*C*), 0.2 (*D*), 0.3 (*E*), 0.4 (*F*), 0.5 (*G*), and 1.0 M (*H*). The *broken lines* are the fitted curves. *I*, CD spectra after aggregation at various concentrations of NaCl. *J*, dependences on the NaCl concentration of the ThT and ANS fluorescence values at 0.5 h and maximum.

NaCl were amorphous aggregates on the basis of AFM and TEM images (8).

We also measured the FTIR spectrum of amorphous aggregates formed in 1.0 M NaCl (Fig. 3*D*). Interestingly, the spectrum showed an altered intermolecular β component around 1616 cm^{-1} and an increased 1634 cm^{-1} peak together with a small but sharp high frequency component, suggesting that the amorphous aggregates contain a large amount of antiparallel β components.

Previously, a similar secondary structure composition was observed for amorphous aggregates of β2m formed at pD 5.5, close to the isoelectric point of the protein (30). It is not rare that amorphous aggregates exhibit high β-sheet content. Among them, Bramanti *et al.* (35) reported β-structured amorphous aggregates of amyloid β-(1–40) peptide induced by ferulic acid, and Arosio *et al.* (36) showed that non-amyloidogenic λ light-chain dimers form amorphous aggregates with increased β-sheet content. In addition, the disagreement between the CD and FTIR results suggests that the extensive precipitation of the aggregates in 1 M NaCl prevented the accurate secondary structure analysis by CD.

The plot of ThT fluorescence against NaCl concentrations showed a maximum at 0.2 M and decreased with a further increase in the NaCl concentration (Fig. 5*J*). Because the slower phase of the two-step increase in ANS fluorescence occurred at the same time range as the increase in ThT fluorescence, it represented the formation of fibrils (Fig. 5*E*). On the other hand, we previously showed that amorphous aggregates formed relatively rapidly without a lag phase (8). Thus, we plotted intensity at 485 nm at 0.5 h, which may represent the amount of amorphous aggregates, and the final maximal value, which represents a sum of the amounts of amyloid fibrils and amorphous aggregates (Fig. 5*J*). ANS fluorescence at 0.5 h increased above 0.2 M NaCl and was saturated at 0.5 M NaCl. The final ANS fluorescence peaked at 0.05 M NaCl and was constant above 0.1 M NaCl. The markedly strong ANS fluorescence at 0.05 M NaCl may have been caused by the electrostatic binding of negatively charged ANS molecules to positively charged β2m fibrils.

Although we assume that oligomers and amorphous aggregates might be continuous as proposed by Miti *et al.* (17), we cannot address the properties of oligomers at this stage because we did not observe oligomers in this study.

Discussion

Competitive Model of Amyloid Fibrillation and Amorphous Aggregation—We proposed a competitive mechanism of amyloid fibrillation and amorphous aggregation to explain NaCl concentration-dependent changes in end products (*Model 2* in Fig. 1*B* and *Mechanism 1* in Fig. 6*A*) (8, 9, 27). A similar competitive mechanism was reported previously for amyloidogenic light chains (37, 38), β2m (39), insulin (40), and α-synuclein (41, 42), in which the aggregation process was branched, with one pathway leading to fibrils and another to oligomeric intermediates that may ultimately form amorphous aggregates. Miti *et al.* (17) recently reported a similar mechanism with hen egg white lysozyme at pH 2 and 52 °C including various stable, metastable, and kinetically trapped amyloid aggregate phases. They focused on transitions from monomers to oligomers, curvilinear fibrils, and oligomeric precipitation and proposed that oligomeric and amorphous aggregates were structurally distinct from rigid fibrils. In addition, they proposed that an experimentally determined phase diagram matches the colloidal model predictions. On the other hand, they considered neither the critical concentration nor supersaturation of amyloid fibrillation. More recently, on the basis of kinetic simulation using an explicit approach, Hall *et al.* (43) suggested possible regulatory effects that off-pathway processes might exert on the rate and extent of amyloid formation.

A long debated issue is whether oligomers or protofibrils represent on-pathway intermediates that must be populated along the pathway leading to fibril formation or off-pathway

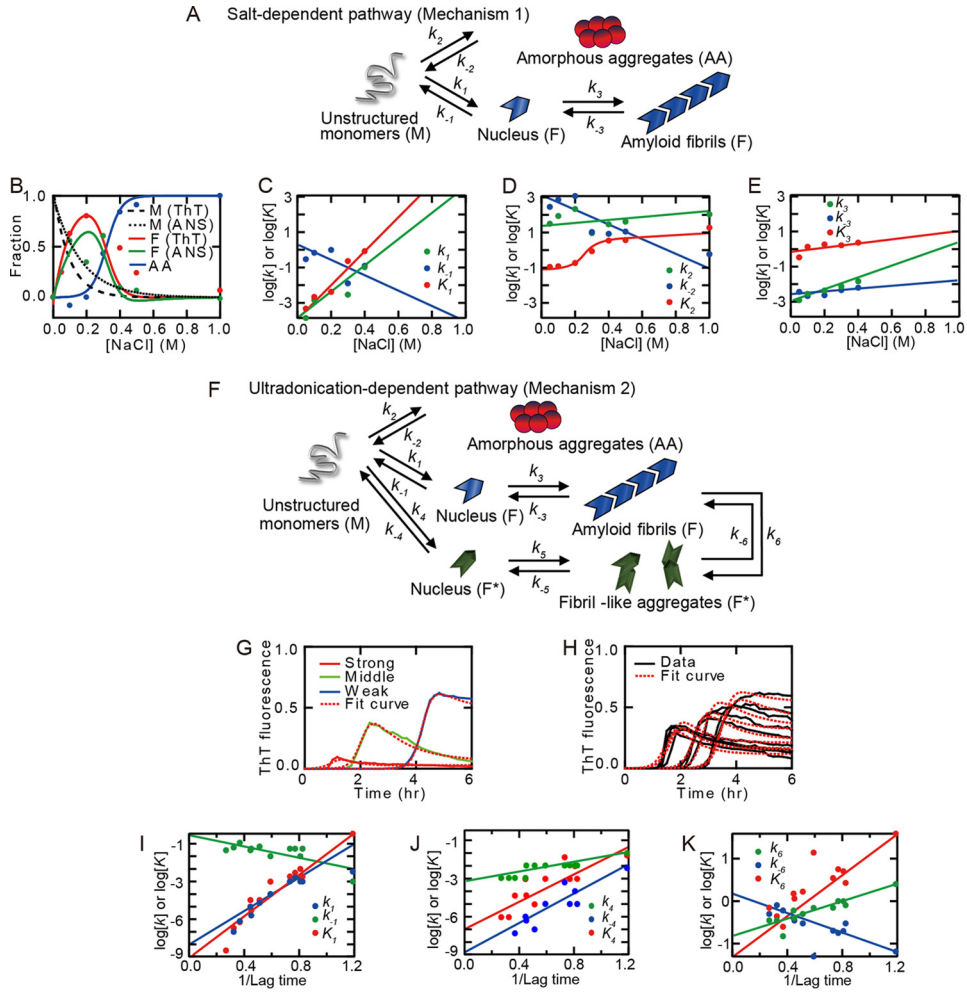

FIGURE 6. **Analysis of the NaCl concentration and the ultrasonic power dependence of amyloid fibrillation by a competitive mechanism.** *A*, the competitive mechanism of amyloid fibrillation and amorphous aggregation. *B*, dependences on the NaCl concentration of the fractions of monomers, fibrils, and amorphous aggregates. *C–E*, dependence on the NaCl concentration of the rate constants and equilibrium constants on the basis of Mechanism 1. *C*, k_1, k_{-1}, and K_1. *D*, k_2, k_{-2}, and K_2. *E*, k_3, k_{-3}, and K_3. *F*, the competitive mechanism of amyloid fibrillation and amorphous aggregation including fibril-like aggregates F*. *G* and *H*, fitting of fibrillation kinetics under various levels of ultrasonic power by the competitive mechanism. *G*, experimental data were the same as those shown in Fig. 2*A*. *H*, experimental data were taken from So *et al.* (22). *I–K*, dependences on the NaCl concentration of rate constants and equilibrium constants on the basis of Mechanism 2. *I*, k_1, k_{-1}, and K_1. *J*, k_4, k_{-4}, and K_4. *K*, k_6, k_{-6}, and K_6. Other rate and equilibrium constants were assumed to be the same as those at 0.1 M NaCl without ultrasonication. *Lines* are guides for the eye.

intermediates that are located at a dead end of the reaction scheme (16) (Fig. 1*B*). The competitive mechanism discussed above supports the off-pathway (or dead end) hypothesis. We previously reported the complete disappearance of the transiently accumulated amorphous aggregates of hen egg white lysozyme or β2m upon amyloid fibrillation, suggesting that amorphous aggregates were also off-pathway products (44, 45). The distinct intermolecular β-sheet component in the infrared spectrum of the amorphous aggregates (1616 cm^{-1} *versus* 1620–1622 cm^{-1} in fibrils, Table 1) suggest a completely different structure and thus further supports the off-pathway hypothesis. On the other hand, many proteins have been shown to form on-pathway oligomers (16). In cases in which oligomers, protofilaments, or amorphous aggregates are off-pathway intermediates, fibrillation occurs only after they dissociate; however, the extent of the conformational change required to restart fibrillation remains largely unknown.

Simulation of Observed Kinetics—We simulated the salt-dependent competition of amyloid fibrillation and amorphous aggregation assuming Mechanism 1 (Fig. 6*A*). In our competitive mechanism, we assumed that all competing processes were reversible with the corresponding critical concentrations. We assumed that amorphous aggregates formed without a lag phase, which is in contrast to the nucleation-limited growth of fibrils (8). Similar competitive and reversible mechanism has been reported for polymers from π-conjugated oligomers, in which two parallel and competing pathways explain the presence of a kinetically favored intermediate assembly that forms quickly but then transforms into a thermodynamically favored form (46). Similar to the competitive mechanism suggested by Miti *et al.* (17), we assumed that our pathway of amorphous aggregation accommodated oligomers, curvilinear fibrils, and large amorphous aggregates, the interconversion of which was more rapid than supersaturation-limited amyloid fibrillation.

To analyze the kinetics of fibrillation on the basis of Mechanism 1, we used equations taken from the F-W model (7).

$$\mathrm{M} \underset{k_{-1}}{\overset{k_1}{\rightleftharpoons}} \mathrm{F} \quad \text{(Eq. 1)}$$

$$\mathrm{M} \underset{k_{-2}}{\overset{k_2}{\rightleftharpoons}} \mathrm{AA} \quad \text{(Eq. 2)}$$

$$\mathrm{M} + \mathrm{F} \underset{k_{-3}}{\overset{k_3}{\rightleftharpoons}} 2\mathrm{F} \quad \text{(Eq. 3)}$$

$$K_1 = \frac{k_1}{k_{-1}} \quad \text{(Eq. 4)}$$

$$K_2 = \frac{k_2}{k_{-2}} \quad \text{(Eq. 5)}$$

and

$$K_3 = \frac{k_3}{k_{-3}} \quad \text{(Eq. 6)}$$

where M is the monomeric protein, F is the amyloid fibril, AA is the amorphous aggregate, k_1, k_{-1}, k_2, k_{-2}, k_3, and k_{-3} represent the rate constants of the respective processes, and K_1, K_2, and K_3 represent the corresponding equilibrium constants. Although these equations considered neither the elongation of fibrils through the ends of fibrils nor the breakage of preformed fibrils, leading to secondary nucleation, we considered them one of the minimal models reproducing the observed kinetics.

To fit the observed kinetics with the model, we estimated the equilibrium (*i.e.* final) fractions of fibrils, amorphous aggregates, and monomers at various salt concentrations. We assumed that 100% of the molecules transformed to amorphous aggregates at 1.0 M NaCl. The fractions of amorphous aggregates at various NaCl concentrations were then estimated from the ANS fluorescence intensity at 0.5 h, when fast amorphous aggregation finished. Analytical ultracentrifuge showed that at concentrations >0.2 M NaCl most of the protein molecules precipitated at 3000 rpm, confirming no significant residual monomers (data not shown). The fractions of fibrils at concentrations >0.2 M NaCl were then obtained by subtracting the fractions of amorphous aggregates from 1. Alternatively, the fractions of fibrils were estimated from the maximal ThT intensities at various NaCl concentrations in which the ThT value at 0.2 N NaCl was used to obtain the specific ThT value of fibrils. In either method the fraction of fibrils showed a maximum at 0.2 M NaCl, whereas the fraction of amorphous aggregates increased at a higher NaCl concentration (Fig. 6*B*).

We fit fast kinetics within 0.5 h, assuming that equilibrium was rapidly established between unfolded monomers and amorphous aggregates. Formation and dissociation rate constants were determined in order to reproduce the fast kinetics and amount of amorphous aggregates at 0.5 h. We then fit the slow kinetics representing the formation of amyloid fibrils. At the respective NaCl concentrations, we assumed a factor relating the ThT fluorescence and ANS fluorescence of fibrils. The fit kinetics showed that the amount of amorphous aggregates exhibited a maximum at moderate concentrations of salt (*e.g.* 0.2–0.3 M NaCl), and this was followed by a slow decrease coupled with the formation of amyloid fibrils. Because ANS fluorescence monitors both amorphous aggregates and amyloid fibrils, it exhibited a shoulder at 0.5 h (Fig. 5, *D* and *E*).

The competitive mechanism sufficiently reproduced the observed kinetics at various NaCl concentrations monitored by ThT and ANS (Fig. 5). Both the equilibrium constants of amyloid nucleation (K_1) (Fig. 6*C*) and amorphous aggregation (K_2) (Fig. 6*D*) increased with higher NaCl concentrations. The equilibrium constant for elongation (K_3) was relatively constant (Fig. 6*E*). However, because amyloid fibrillation was more favorable before amorphous aggregation became dominant, the maximum amount of fibrils was achieved at moderate concentrations of NaCl (Fig. 6*B*).

Free Energy Change of Protein Aggregation and Phase Diagram—Although the detailed mechanisms of protein aggregation remain elusive (7), a simplified model on the basis of the equilibrium of monomers and aggregated forms proposes the importance of the remaining monomer concentration $[\mathrm{M}]_c$, which is often referred to as the "critical concentration" (5, 6, 12, 47, 48) because aggregates form when the concentration of monomers exceeds $[\mathrm{M}]_c$. By determining $[\mathrm{M}]_c$, we can calculate the free energy change in fibrillation or amorphous aggregation ($\Delta G_{\mathrm{M\text{-}F}}$ or $\Delta G_{\mathrm{M\text{-}AA}}$) by $\Delta G = -RT\ln K = RT\ln[\mathrm{M}]_c$, where R and T are the gas constant and temperature, respectively. Critical concentration is analogous to critical micelle concentration and is an important parameter independent of the complicated mechanisms of aggregation. Moreover, when we assume a phase transition between monomers and solid-like fibrils or amorphous aggregates, $[\mathrm{M}]_c$ simply represents the solubility of monomers.

The salt-dependent phase transitions of the major products, from monomers to amyloid fibrils to amorphous aggregates, can be illustrated by NaCl concentration-dependent changes in the $[\mathrm{M}]_c$ values for amyloid fibrils and amorphous aggregates (Fig. 7). The logarithm of the $[\mathrm{M}]_c$ value is proportional to the standard free energy change in the phase transition (Fig. 7*A*). At NaCl concentrations lower than ~0.05 M, the $[\mathrm{M}]_c$ values of amorphous aggregation and amyloid fibrillation were both higher than the experimental protein concentration (25 μM or 0.3 mg/ml); therefore, the free energy changes of aggregation were positive (*Region 1*). Thus, monomers dominated in equilibrium. At a NaCl concentration between 0.05 and 0.15 M (*Region 2a*), the free energy change of amyloid fibrillation became negative, whereas that of amorphous aggregation was still positive. Thus, only amyloid fibrillation occurred after a lag phase. At a NaCl concentration between 0.15 and ~0.3 M (*Region 2b*), free energy change of amorphous aggregation became negative. Because amorphous aggregation is rapid and amyloid fibrillation is slow, the rapid formation and slow relaxation of amorphous aggregation was coupled with the slow formation of amyloid fibrils (Fig. 7*C*). Only the rapid formation of amorphous aggregates occurred at a NaCl concentration >~0.5 M. Here, it is noted that Region 2 (amyloid fibrils) in the general phase diagram shown in Fig. 1*A* was divided into two subregions (*Regions 2a* and *2b*) depending on the kinetics of fibrillation.

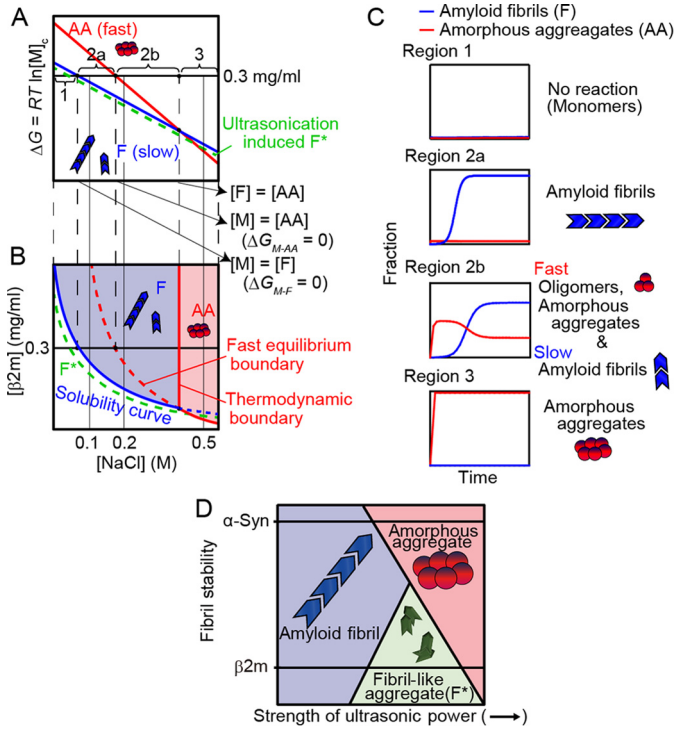

FIGURE 7. **Competitive mechanism of supersaturation-limited and unlimited reactions.** *A*, dependences on the NaCl concentration of free energy changes of amyloid fibrillation and amorphous aggregation. The *solid horizontal line* indicates free energy changes for phase transitions at the β2m concentration (25 μM). *Region 1*, critical concentrations for fibrillation and amorphous aggregations were higher than the β2m concentration in the solution. *Region 2a*, critical concentrations for fibrillation and amorphous aggregations were lower and higher, respectively, than the β2m concentration. *Region 2b*, critical concentrations for fibrillation and amorphous aggregations were both lower than the β2m concentration, with the former being lower than the latter. *Region 3*, after the crossing point, the critical concentration of amorphous aggregation was lower than that of fibrillation and, thus, determined the overall kinetics. *B*, the protein concentration- and NaCl concentration-dependent phase diagram of conformational states. The *dotted green lines* in *A* and *B* indicate the possible free energy profile and phase boundary, respectively, for the transition from monomers to F* fibrils under the conditions of extensive ultrasonication. *C*, representative kinetics under *Regions 1–3* are illustrated. *D*, dependence of the effects of ultrasonication on the stability of amyloid fibrils. Stable fibrils like those of β2m produced partially destructed fibrillar aggregates, whereas less stable α-synuclein fibrils exhibited two-state destruction by ultrasonic irradiation.

Moreover, salt-dependent changes in the fit rates and equilibrium constants of fibrillation and amorphous aggregation suggested the origin of the observed complicated kinetics (Fig. 6, *C–E*). The increase in fibrillation equilibrium (K_1, K_3) was mainly caused by an elevated nucleation rate (k_1) (Fig. 6*C*) without a significant change in the elongation reaction (Fig. 6*E*). On the other hand, the increase in amorphous aggregation (K_2) was caused by a decrease in the dissociation rate (k_{-2}) (Fig. 6*D*).

The observed kinetics of amyloid fibrillation also illustrate the conformational phase diagram, which is dependent on NaCl and protein concentrations (Fig. 7*B*). Although the linear dependences of the free energy changes of amyloid fibrillation and amorphous aggregation with a crossing point at a high NaCl concentration predicted the disappearance of an amyloidogenic region at the low protein concentration and high NaCl concentration regions, the exact shape of the phase diagram under the extreme protein and salt concentrations remain unknown without exact data under those conditions. In this context it is noted that a general phase diagram shown in Fig. 1*A* assumed the persistence of amyloidogenic region even at very high salt concentrations. Nevertheless, we argue that a conformational phase diagram common to various amyloidogenic proteins may be reproduced by a competitive mechanism between supersaturation-limited amyloid fibrillation and unlimited amorphous aggregation.

Ultrasonication-dependent Decrease in ThT Fluorescence—In the cases of α-synuclein (27) and amyloid β peptides (26), extensive ultrasonication transformed preformed fibrils to amorphous aggregates with decreased ThT fluorescence, as confirmed by a CD spectroscopy and EM or AFM images. This was not the case for β2m fibrils and fibrillar aggregates with reduced ThT fluorescence that retained amyloid-like β-structures. Similar aggregates were induced from β2m monomers under extensive ultrasonic power (Figs. 2 and 3).

We now assume that extensive ultrasonication can produce a distinct conformational state located between amorphous aggregates and amyloid fibrils, which may be represented by F* (Fig. 6*F*, *Mechanism 2*). We modified Mechanism 1 by adding an additional pathway producing F* (Equations 7 and 8). We also assumed that the preformed fibrils (F) may be converted to (F*) by extensive ultrasonication (Equation 9),

$$M \underset{k_{-4}}{\overset{k_4}{\rightleftharpoons}} F^* \qquad \text{(Eq. 7)}$$

$$M + F \underset{k_{-5}}{\overset{k_5}{\rightleftharpoons}} 2F^* \qquad \text{(Eq. 8)}$$

$$F \underset{k_{-6}}{\overset{k_6}{\rightleftharpoons}} F^* \qquad \text{(Eq. 9)}$$

$$K_4 = \frac{k_4}{k_{-4}} \qquad \text{(Eq. 10)}$$

$$K_5 = \frac{k_5}{k_{-5}} \qquad \text{(Eq. 11)}$$

and

$$K_6 = \frac{k_6}{k_{-6}} \qquad \text{(Eq. 12)}$$

With these equations on the basis of Mechanism 2 (Fig. 6*F*), a series of kinetic data as shown in Fig. 2 were simulated in which ultrasonic power varied at 0.1 M NaCl (Fig. 6*G*). Moreover, we analyzed a series of data obtained by So *et al.* (22) with a microplate in which ultrasonic power varied depending on the wells of the microplate (Fig. 6*H*). In an analysis of ultrasonication-dependent reactions, we assumed that the rate (k_2, and k_{-2} (Equation 2)) and equilibrium constants (K_2 (Equation 5)) of amorphous aggregates and those for elongation processes of amyloid fibrils (k_3, and k_{-3} (Equation 3) and K_3 (Equation 6)) and amyloid-like fibrils (k_5, k_{-5} (Equation 8), and K_5 (Equation 11)) were

the same as those obtained for stirring-dependent reactions at 0.1 M NaCl because they are unlikely to be significantly affected by ultrasonication (8).

All the observed kinetics were reproduced successfully, suggesting that the competitive mechanism was also useful for explaining the dependence on ultrasonic power of the kinetics monitored by ThT; however, β2m retained an amyloid-like β structure even after extensive ultrasonication. Under the conditions of stronger ultrasonic power, the population of fibrils decreased, whereas that of modified fibrils became dominant because the modified fibrils were favored kinetically and the preformed fibrils transformed to modified fibrils by extensive ultrasonication (Fig. 6, *G* and *H*). The possible free energy profile and phase diagram for the formation of F* fibrils under the conditions of extensive ultrasonication are illustrated in Fig. 7, *A* and *B*.

The inverse of lag time was considered to represent ultrasonic power. K_1, k_1, and k_{-1} (Fig. 6*I*), K_4, k_4, and k_{-4} (Fig. 6*J*), and K_6, k_6, and k_{-6} (Fig. 6*K*) were then plotted against the inverse of lag time. The parameters obtained suggested that the combined effects of the equilibrium and rate toward the formation of F* explain the accumulation of F* under stronger ultrasonic powers. Although the significance of the respective rate constants still remains unclear, we adequately reproduced the change in the kinetics of fibrillation on the basis of competition between the parallel pathways (Fig. 6*F*).

Conclusion—Competition between crystallization and glass transition has been elaborated for understanding the mechanism of protein folding (29, 31, 49), in which the folding temperature (T_f) corresponded to the temperature of crystallization and the glass transition temperature (T_g) resembled the temperature of amorphous aggregation in which molecules were trapped in various local minima. To achieve cooperative and rapid protein folding, the temperature of glass transition should be markedly lower than the folding temperature in order to construct a smooth folding funnel with minimal frustration. An analogy of protein phase transition into crystal-like amyloid fibrils and amorphous aggregates appears to be valid. In the case of salt-dependent fibrillation, the critical concentrations of amyloid fibrils and amorphous aggregates (or oligomers) correspond to the folding temperature and glass transition temperature, respectively. To achieve cooperative amyloid fibrillation, two critical concentrations need to be markedly separated. However, for larger denatured proteins, the critical concentration of amorphous aggregation was close to that of fibrillation, making amyloid fibrillation difficult. In other words the free energy balance between amyloid fibrils and amorphous aggregates determines their final distributions.

In addition, the current analysis argued the importance of supersaturation. Although we approximated amyloid fibrillation by a nucleation and growth mechanism, supersaturation is often too rigid to be broken under quiescent conditions. One possibility underlying spontaneous fibrillation under labile region is that supersaturation-unlimited amorphous aggregates gradually develop with an increase in the driving force of precipitation (*e.g.* NaCl concentration), thereby providing the seed-competent structures and ultimately breaking otherwise persistent supersaturation.

Finally, although oligomers are important targets of protein aggregation, we could not focus on them because we did not isolate them clearly. Characterizing the exact role of oligomers in the context of the competitive mechanism will be important for further clarifying the general mechanism of protein aggregation.

Author Contributions—M. A. and J. K. performed experiments. M. A., M. S., and K. S. analyzed data. M. A., M. S., and Y. G. designed experiments and wrote the manuscript.

Acknowledgments—We thank Damien Hall (Australian National University) and Hirotsugu Ogi (Osaka University) for critical discussions. We thank Elemér Vass (Eötvös University) for providing the FTIR machine for the experiments.

References

1. Chiti, F., and Dobson, C. M. (2006) Protein misfolding, functional amyloid, and human disease. *Annu. Rev. Biochem.* **75,** 333–366
2. Eisenberg, D., and Jucker, M. (2012) The amyloid state of proteins in human diseases. *Cell* **148,** 1188–1203
3. Tycko, R., and Wickner, R. B. (2013) Molecular structures of amyloid and prion fibrils: consensus versus controversy. *Acc. Chem. Res.* **46,** 1487–1496
4. Sipe, J. D., Benson, M. D., Buxbaum, J. N., Ikeda, S., Merlini, G., Saraiva, M. J., and Westermark, P. (2014) Nomenclature 2014: amyloid fibril proteins and clinical classification of the amyloidosis. *Amyloid* **21,** 221–224
5. Jarrett, J. T., and Lansbury, P. T., Jr. (1993) Seeding "one-dimensional crystallization" of amyloid: a pathogenic mechanism in Alzheimer's disease and scrapie? *Cell* **73,** 1055–1058
6. Wetzel, R. (2006) Kinetics and thermodynamics of amyloid fibril assembly. *Acc. Chem. Res.* **39,** 671–679
7. Morris, A. M., Watzky, M. A., and Finke, R. G. (2009) Protein aggregation kinetics, mechanism, and curve-fitting: a review of the literature. *Biochim. Biophys. Acta* **1794,** 375–397
8. Yoshimura, Y., Lin, Y., Yagi, H., Lee, Y. H., Kitayama, H., Sakurai, K., So, M., Ogi, H., Naiki, H., and Goto, Y. (2012) Distinguishing crystal-like amyloid fibrils and glass-like amorphous aggregates from their kinetics of formation. *Proc. Natl. Acad. Sci. U.S.A.* **109,** 14446–14451
9. Kitayama, H., Yoshimura, Y., So, M., Sakurai, K., Yagi, H., and Goto, Y. (2013) A common mechanism underlying amyloid fibrillation and protein crystallization revealed by the effects of ultrasonication. *Biochim. Biophys. Acta* **1834,** 2640–2646
10. Lin, Y., Lee, Y. H., Yoshimura, Y., Yagi, H., and Goto, Y. (2014) Solubility and supersaturation-dependent protein misfolding revealed by ultrasonication. *Langmuir* **30,** 1845–1854
11. Muta, H., Lee, Y. H., Kardos, J., Lin, Y., Yagi, H., and Goto, Y. (2014) Supersaturation-limited amyloid fibrillation of insulin revealed by ultrasonication. *J. Biol. Chem.* **289,** 18228–18238
12. Ikenoue, T., Lee, Y. H., Kardos, J., Yagi, H., Ikegami, T., Naiki, H., and Goto, Y. (2014) Heat of supersaturation-limited amyloid burst directly monitored by isothermal titration calorimetry. *Proc. Natl. Acad. Sci. U.S.A.* **111,** 6654–6659
13. Hofrichter, J., Ross, P. D., and Eaton, W. A. (1976) Supersaturation in sickle cell hemoglobin solutions. *Proc. Natl. Acad. Sci. U.S.A.* **73,** 3035–3039
14. Eaton, W. A., and Hofrichter, J. (1987) Hemoglobin S gelation and sickle cell disease. *Blood* **70,** 1245–1266
15. Ciryam, P., Tartaglia, G. G., Morimoto, R. I., Dobson, C. M., and Vendruscolo, M. (2013) Widespread aggregation and neurodegenerative diseases are associated with supersaturated proteins. *Cell Rep.* **5,** 781–790
16. Bemporad, F., and Chiti, F. (2012) Protein misfolded oligomers: Experimental approaches, mechanism of formation, and structure-toxicity relationships. *Chem. Biol.* **19,** 315–327
17. Miti, T., Mulaj, M., Schmit, J. D., and Muschol, M. (2015) Stable, metasta-

ble, and kinetically trapped amyloid aggregate phases. *Biomacromolecules* **16,** 326–335
18. Platt, G. W., Routledge, K. E., Homans, S. W., and Radford, S. E. (2008) Fibril growth kinetics reveal a region of β2-microglobulin important for nucleation and elongation of aggregation. *J. Mol. Biol.* **378,** 251–263
19. Giehm, L., and Otzen, D. E. (2010) Strategies to increase the reproducibility of protein fibrillization in plate reader assays. *Anal. Biochem.* **400,** 270–281
20. Ohhashi, Y., Kihara, M., Naiki, H., and Goto, Y. (2005) Ultrasonication-induced amyloid fibril formation of β2-microglobulin. *J. Biol. Chem.* **280,** 32843–32848
21. Chatani, E., Lee, Y. H., Yagi, H., Yoshimura, Y., Naiki, H., and Goto, Y. (2009) Ultrasonication-dependent production and breakdown lead to minimum-sized amyloid fibrils. *Proc. Natl. Acad. Sci. U.S.A.* **106,** 11119–11124
22. So, M., Yagi, H., Sakurai, K., Ogi, H., Naiki, H., and Goto, Y. (2011) Ultrasonication-dependent acceleration of amyloid fibril formation. *J. Mol. Biol.* **412,** 568–577
23. Yoshimura, Y., So, M., Yagi, H., and Goto, Y. (2013) Ultrasonication: an efficient agitation for accelerating the supersaturation-limited amyloid fibrillation of proteins. *Jpn. J. Appl. Phys.* **52,** 1–8
24. Yamaguchi, K., Matsumoto, T., and Kuwata, K. (2012) Proper calibration of ultrasonic power enabled the quantitative analysis of the ultrasonication-induced amyloid formation process. *Protein Sci.* **21,** 38–49
25. Umemoto, A., Yagi, H., So, M., and Goto, Y. (2014) High-throughput analysis of the ultrasonication-forced amyloid fibrillation reveals the mechanism underlying the large fluctuation in the lag time. *J. Biol. Chem.* **289,** 27290–27299
26. Yagi, H., Hasegawa, K., Yoshimura, Y., and Goto, Y. (2013) Acceleration of the depolymerization of amyloid β fibrils by ultrasonication. *Biochim. Biophys. Acta* **1834,** 2480–2485
27. Yagi, H., Mizuno, A., So, M., Hirano, M., Adachi, M., Akazawa-Ogawa, Y., Hagihara, Y., Ikenoue, T., Lee, Y. H., Kawata, Y., and Goto, Y. (2015) Ultrasonication-dependent formation and degradation of α-synuclein amyloid fibrils. *Biochim. Biophys. Acta* **1854,** 209–217
28. Chiba, T., Hagihara, Y., Higurashi, T., Hasegawa, K., Naiki, H., and Goto, Y. (2003) Amyloid fibril formation in the context of full-length protein: effects of proline mutations on the amyloid fibril formation of β2-microglobulin. *J. Biol. Chem.* **278,** 47016–47024
29. Nymeyer, H., García, A. E., and Onuchic, J. N. (1998) Folding funnels and frustration in off-lattice minimalist protein landscapes. *Proc. Natl. Acad. Sci. U.S.A.* **95,** 5921–5928
30. Kardos, J., Okuno, D., Kawai, T., Hagihara, Y., Yumoto, N., Kitagawa, T., Závodszky, P., Naiki, H., and Goto, Y. (2005) Structural studies reveal that the diverse morphology of β2-microglobulin aggregates is a reflection of different molecular architectures. *Biochim. Biophys. Acta* **1753,** 108–120
31. Bryngelson, J. D., Onuchic, J. N., Socci, N. D., and Wolynes, P. G. (1995) Funnels, pathways, and the energy landscape of protein folding: a synthesis. *Proteins* **21,** 167–195
32. Bouchard, M., Zurdo, J., Nettleton, E. J., Dobson, C. M., and Robinson, C. V. (2000) Formation of insulin amyloid fibrils followed by FTIR simultaneously with CD and electron microscopy. *Protein Sci.* **9,** 1960–1967
33. Goto, Y., and Fink, A. L. (1989) Conformational state of β-lactamase: molten-globule states at acidic and alkaline pH with high salt. *Biochemistry* **28,** 945–952
34. Raman, B., Chatani, E., Kihara, M., Ban, T., Sakai, M., Hasegawa, K., Naiki, H., Rao, Ch. M., and Goto, Y. (2004) Critical balance of charge interactions is required for β2-microglobulin amyloid fibril growth and stability: influence by co-solute anions. *Biochemistry* **44,** 1288–1299
35. Bramanti, E., Fulgentini, L., Bizzarri, R., Lenci, F., and Sgarbossa, A. (2013) β-Amyloid amorphous aggregates induced by the small natural molecule ferulic acid. *J. Phys. Chem. B* **117,** 13816–13821
36. Arosio, P., Owczarz, M., Müller-Späth, T., Rognoni, P., Beeg, M., Wu, H., Salmona, M., and Morbidelli, M. (2012) In vitro aggregation behavior of a non-amyloidogenic λ light chain dimer deriving from U266 multiple myeloma cells. *PLoS ONE* **7,** e33372
37. Souillac, P. O., Uversky, V. N., Millett, I. S., Khurana, R., Doniach, S., and Fink, A. L. (2002) Elucidation of the molecular mechanism during the early events in immunoglobulin light chain amyloid fibrillation: evidence for an off-pathway oligomer at acidic pH. *J. Biol. Chem.* **277,** 12666–12679
38. Souillac, P. O., Uversky, V. N., and Fink, A. L. (2003) Structural transformations of oligomeric intermediates in the fibrillation of the immunoglobulin light chain LEN. *Biochemistry* **42,** 8094–8104
39. Gosal, W. S., Morten, I. J., Hewitt, E. W., Smith, D. A., Thomson, N. H., and Radford, S. E. (2005) Competing pathways determine fibril morphology in the self-assembly of β2-microglobulin into amyloid. *J. Mol. Biol.* **351,** 850–864
40. Hong, D. P., Ahmad, A., and Fink, A. L. (2006) Fibrillation of human insulin A and B chains. *Biochemistry* **45,** 9342–9353
41. Dusa, A., Kaylor, J., Edridge, S., Bodner, N., Hong, D. P., and Fink, A. L. (2006) Characterization of oligomers during α-synuclein aggregation using intrinsic tryptophan fluorescence. *Biochemistry* **45,** 2752–2760
42. Uversky, V. N., and Eliezer, D. (2009) Biophysics of parkinson's disease: structure and aggregation of α-synuclein. *Curr. Protein Pept. Sci.* **10,** 483–499
43. Hall, D., Kardos, J., Edskes, H., Carver, J. A., and Goto, Y. (2015) A multipathway perspective on protein aggregation: implications for control of the rate and extent of amyloid formation. *FEBS Lett.* **589,** 672–679
44. Sasahara, K., Yagi, H., Naiki, H., and Goto, Y. (2007) Heat-induced conversion of β2-microglobulin and hen egg-white lysozyme into amyloid fibrils. *J. Mol. Biol.* **372,** 981–991
45. Sasahara, K., Yagi, H., Sakai, M., Naiki, H., and Goto, Y. (2008) Amyloid nucleation triggered by agitation of β2-microglobulin under acidic and neutral pH conditions. *Biochemistry* **47,** 2650–2660
46. Korevaar, P. A., George, S. J., Markvoort, A. J., Smulders, M. M., Hilbers, P. A., Schenning, A. P., De Greef, T. F., and Meijer, E. W. (2012) Pathway complexity in supramolecular polymerization. *Nature* **481,** 492–496
47. Kardos, J., Yamamoto, K., Hasegawa, K., Naiki, H., and Goto, Y. (2004) Direct measurement of the thermodynamic parameters of amyloid formation by isothermal titration calorimetry. *J. Biol. Chem.* **279,** 55308–55314
48. Kardos, J., Micsonai, A., Pál-Gábor, H., Petrik, É., Gráf, L., Kovács, J., Lee, Y. H., Naiki, H., and Goto, Y. (2011) Reversible heat-induced dissociation of β2-microglobulin amyloid fibrils. *Biochemistry* **50,** 3211–3220
49. Wolynes, P. G. (2005) Energy landscapes and solved protein-folding problems. *Philos. Trans. A. Math. Phys. Eng. Sci.* **363,** 453–464